



HAL
open science

The crucial impact of cerium reduction on photoluminescence

Romain Génois, Stéphane Jobic, Guy Ouvrard, Florian Massuyeau, Romain Gautier

► **To cite this version:**

Romain Génois, Stéphane Jobic, Guy Ouvrard, Florian Massuyeau, Romain Gautier. The crucial impact of cerium reduction on photoluminescence. *Applied Materials Today*, 2020, 20, pp.100643. 10.1016/j.apmt.2020.100643 . hal-02993325

HAL Id: hal-02993325

<https://hal.science/hal-02993325>

Submitted on 13 Nov 2020

HAL is a multi-disciplinary open access archive for the deposit and dissemination of scientific research documents, whether they are published or not. The documents may come from teaching and research institutions in France or abroad, or from public or private research centers.

L'archive ouverte pluridisciplinaire **HAL**, est destinée au dépôt et à la diffusion de documents scientifiques de niveau recherche, publiés ou non, émanant des établissements d'enseignement et de recherche français ou étrangers, des laboratoires publics ou privés.

The Crucial Impact of Cerium Reduction on Photoluminescence

Romain Génois,¹ Stéphane Jobic,¹ Guy Ouvrard,¹ Florian Massuyeau,¹ and Romain Gautier^{1,*}

¹Centre National de la Recherche Scientifique CNRS-IMN, 2 rue de la Houssinière, 44300 Nantes, France

ABSTRACT

Rare earth-based inorganic phosphors are of great interest for solid-state lighting because some of them present very efficient luminescence properties. However, their performances strongly depend on several parameters. For multivalent dopants such as cerium, a widely used activator in the lighting industry, a synthesis in reducing atmosphere is often required to stabilize the dopant in its lower oxidation state. Surprisingly, this crucial step is not much considered, and the presence of the reduced state only is often assumed. However, the presence of the dopants oxidized form has been previously evidenced after such reductions. In this case, a question remains open about the impact of the $\text{Ce}^{3+}/\text{Ce}^{4+}$ ratio on the materials optical properties. As an example, different $\text{CaSc}_2\text{O}_4:\text{Ce}$ samples were prepared and their $\text{Ce}^{3+}/\text{Ce}^{4+}$ ratios were probed by diffuse reflection and XANES. The evolution of their photoluminescence properties was investigated to rationalize the progressive reduction of dopants.

Keywords: Cerium, doping, luminescence, reduction, solid-state lighting

1. Introduction

The solid-state lighting industry is in constant growth,[1] and the annual sales revenue for Light-Emitting Diodes (LEDs) applications is expected to reach 20 billion \$ in 2021.[2] This growth originates from an extended use of LEDs in every lighting market (e.g. automobile, house and public lighting) leading to energy savings expected at 75% by 2035.[2][3] In this context, rare earth-doped phosphors are of great interest for phosphor-converted LEDs. Cerium-doped phosphors are widely studied because they present some of the most efficient luminescence properties. For example, some materials exhibit very high Photoluminescence Quantum Yield (PLQY) as the commercially available $\text{Y}_3\text{Al}_5\text{O}_{12}:\text{Ce}$ (YAG:Ce, PLQY > 90%[4][5]), used for LEDs and Hg-free lamps for instance, or $\text{Sr}_{2.975-x}\text{Ba}_x\text{Ce}_{0.025}\text{AlO}_4\text{F}$ (PLQY \approx 100%[6]). Some phosphors also present very high luminescence thermal stabilities with high PLQY such as $\text{Ca}_3\text{Sc}_2\text{Si}_3\text{O}_{12}:\text{Ce}$ (CSSO:Ce[7,8]).

So far, reaching and reproducing such performances remain challenging because they depend on many parameters, sometimes difficult to control, such as dopant concentration, homogeneity of the activator dispersion, synthesis temperature, grain size or crystallinity. For multivalent dopants (e.g. Ce, Eu or Mn) a reduction is also often required. For cerium this step clearly aims at stabilizing the luminescent Ce^{3+} instead of the commonly non-luminescent Ce^{4+} . Even though, the possible coexistence of the two oxidations states of the dopant is not much considered, and a single state of the activator only is often expected to be stabilized. However, even under severe reducing conditions, a mixed valence may exist. Thus, Wang et al. showed by XPS the presence of Ce^{4+} in YAG:Ce after such strong reductions.[9] Moreover, reduction conditions have been reported to greatly increase the luminescence intensity of YAG:Ce and CSSO:Ce.[10][11] Furthermore, the stabilization of several oxidation states by soft reduction routes has been referenced to allow luminescence or absorption tuning.[12–14] Therefore, an overall question remains open on the properties reproducibility if full reduction under strong conditions is not reached. In this context, in order to investigate partial reduction more thoroughly, we propose here the study of $\text{CaSc}_2\text{O}_4:\text{Ce}$ and the impact of the Ce^{3+} ratio (percentage of Ce^{3+} over the whole cerium amount) on the material photoluminescence properties. This phosphor shows drastic luminescence efficiency changes with slight Ce^{3+} concentration modifications.[15] This phenomenon makes $\text{CaSc}_2\text{O}_4:\text{Ce}$ a good candidate to study the impact of the Ce^{3+} ratio on its luminescent properties while significant changes can be expected.

2. Material and Methods

Combustion syntheses may be highly exothermic. Proper safety measures should be taken.

All samples were synthesized by combustion method and according to the following formulas: $\text{Ca}_{0.9925}\text{Sc}_2\text{O}_4:0.005\text{Ce}$ and $\text{Ca}_{0.97}\text{Sc}_2\text{O}_4:0.015\text{Ce}$. The starting materials CaCO_3 (Merck, 99.5%), $\text{ScCl}_3 \cdot 6\text{H}_2\text{O}$ (Alfa

* Corresponding author. e-mail: romain.gautier@cnsr-immn.fr.

Aesar, 99.9%) and $\text{Ce}(\text{NO}_3)_3 \cdot 6\text{H}_2\text{O}$ (Alfa Aesar, 99.99%) were first dissolved in nitric acid (65%) and kept under stirring at room temperature until formation of a colorless solution. Then, Glycine (Sigma Aldrich, 98%) was added. The mixture was kept under stirring until complete dissolution of glycine, and then heated until combustion. The obtained product was then ground in an agate mortar, placed in an alumina crucible, and fired at 1000°C in air for 1h in a muffle furnace. The samples synthesized in reducing atmosphere were fired at 1000°C under 0.3L/min 5% H_2 /95%Ar gas flow in an alumina tube furnace. Powder X-ray diffraction patterns were collected using a Bruker Axis DS diffractometer for 1h from 5° to 90° with a 0.02° step size. Rietveld refinements were carried out using JANA-2006. All parameters have been refined, including the atomic isotropic displacement. Diffuse reflection spectra were collected with a Perkin Elmer Lambda 1050 device equipped with a 150 mm integration sphere. Solid-state photoluminescence spectra were obtained at room temperature with a Jobin-Yvon Fluorolog 3 spectrophotometer using a xenon lamp (450 W) and a photomultiplier tube (PMT) R13456 from Hamamatsu. Photoluminescence Quantum Yield (PLQY) measurements were recorded using the de Mello method,[16] at room temperature with a Horiba quanta-phi integrating sphere optically connected with the Fluorolog 3 through fibers. PLQY of standard sample SGA 550 100 Isiphor from Sigma Aldrich was measured at 90%. XANES experiments on our materials at the Ce-L_{III} (5724 eV) edge were carried out in the fluorescence detection mode at Synchrotron SOLEIL on the Samba beamline. Spectra normalization, absorption edges treatment and linear combination fits were realized using ATHENA.[17] EXAFS experiments were carried out at the Ce-K edge (40444 eV) in the transmission mode at Synchrotron SOLEIL on the Rock beamline equipped with a Quick-EXAFS setup monochromator. The extraction of EXAFS signals and their treatments were realized using the WinXAS software.[18]

3. Results and discussion

CaSc_2O_4 crystallizes in the CaFe_2O_4 type (orthorhombic system (*Pnam*)) with one type of 8-coordinated Ca^{2+} and two independent 6-coordinated Sc^{3+} sites defining distorted ScO_6 octahedra. Ce^{3+} cations are referenced to substitute Ca^{2+} sites ($r(\text{Ce}^{3+}) = 1.28 \text{ \AA}$, $r(\text{Ca}^{2+}) = 1.26 \text{ \AA}$) and are at the origin of a broad green emission under excitation at 445 nm.[15] This emission can be deconvoluted into two bands peaking at 479 nm (2.59 eV) and 525 nm (2.36 eV) (maximum at 517 nm, 0.25 eV separation, see Fig. S1) and assigned to $5d^1 \rightarrow {}^2F_{5/2}$ and $5d^1 \rightarrow {}^2F_{7/2}$ transitions of Ce^{3+} at the Ca site. $\text{CaSc}_2\text{O}_4:\text{Ce}$ presents high PLQY of 85% at room temperature with a very low dopant concentration of 0.5%.[15] Moreover, $\text{CaSc}_2\text{O}_4:\text{Ce}$ shows drastic efficiency changes with slight Ce concentration modifications. Thereby, its PLQY drops sharply from 85% to 31% between samples doped with 0.5% and 1.5% respectively.[15] In order to study the impact of the reducing treatment on $\text{CaSc}_2\text{O}_4:\text{Ce}$, a series of five samples doped with 0.5% of cerium has been prepared by combustion method. The powder samples were fired at 1000°C either in air for 1h (CSO-0) or under Ar/ H_2 (95/5) flow for durations ranging from 1h to 96h (CSO-1, 24, 48 and 96). In parallel, two samples doped with 1.5% of cerium were prepared by combustion method and fired at 1000°C for 1h in air. One sample did not undergo any further treatment (CSO-1.5-0). The second sample was annealed several times at 1000°C for 1h under Ar/ H_2 (95/5) flow (CSO-1.5-red).

Powder X-ray diffraction (PXRD) and Rietveld refinements confirmed that all samples were obtained pure (see Fig 1(a) for CSO-24, and Fig. S2 for all the other samples). Moreover, no significant differences have been noticed regarding to the samples microstructures. PXRD patterns show no significant differences in peaks width between the samples reduced from 24h to 96h (Fig. S3) as well as in their cell parameters obtained by Rietveld refinement (Table S1).

Diffuse reflection has been proved to be an appropriate tool to probe the presence of Ce^{3+} in CaSc_2O_4 .[19] In this context, the spectra of samples CSO-0 to CSO-96 were collected (Fig. 1(b)). In addition to an absorption band below 400 nm, the reduced samples present a new absorption band, compared to CSO-0, centered at 445 nm. This band, corresponding to the material maximum of excitation,[15,19] presents a continuous increase with the reduction duration and a stabilization of its intensity between CSO-48 and CSO-96. This band is correlated to the presence of Ce^{3+} [19] and confirms the increase of the Ce^{3+} ratio with reduction. Moreover, the absence of band at 445 nm for the non-reduced sample (CSO-0) suggests that Ce^{3+} cations are not present in this sample (at least at the detection threshold of the technique), implying a sample mainly doped with Ce^{4+} . The observed

stabilization of the intensity of the band at 445 nm between CSO-48 and CSO-96, supposes that CSO-96 is fully reduced and so only doped with Ce^{3+} (or at least containing the largest Ce^{3+} ratio reachable by reduction). Therefore, CSO-1 to CSO-48 might present different Ce^{3+} ratios, continuously increasing with the reduction duration. The absorption band below 400 nm has been previously attributed to $4f \rightarrow 5d$ Ce^{3+} transitions.[19] However, the slightly shift in position of this band for all samples and its presence for the non-reduced sample (expected to be fully Ce^{4+} -doped),

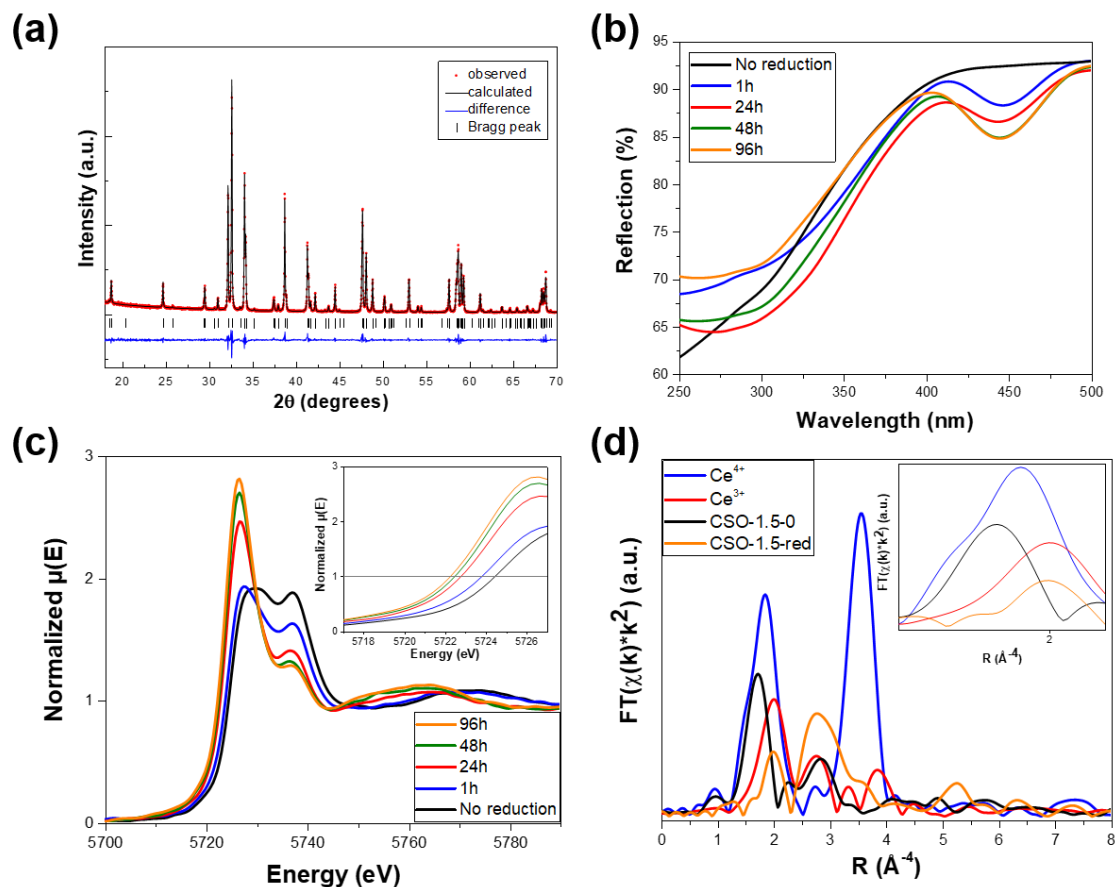


Fig. 1. (a) PXRD pattern and Rietveld refinement of CSO-24.[20] (b) Diffuse reflection spectra and (c) Normalized L3 XANES spectra for samples CSO-0 to CSO-96. (d) Radial distribution functions of the Ce^{4+} standard (CeO_2 , blue line), the Ce^{3+} standard ($\text{CePO}_4 \cdot 0.5\text{H}_2\text{O}$, red line), the non-reduced sample (black line) and the strongly reduced sample (orange line).

make this attribution questionable. A $\text{O}^{2-} \rightarrow \text{Sc}^{3+}$ charge transfer could be assumed but the undoped CaSc_2O_4 is reported without absorption threshold above 260 nm.[19] The absorption at 400 nm, present for the non-reduced and all the reduced samples, could then be associated to a O^{2-} - Ce^{4+} transition as proposed by Goubin et al[21].

XANES measurements at the cerium L3 edge have been carried out as a local probe of the Ce^{3+} ratio, the presence of Ce^{4+} and Ce^{3+} being characterized by bands respectively at 5737 eV and 5726 eV.[22,23] XANES spectra of the Ce^{4+} and Ce^{3+} standards, respectively CeO_2 and $\text{CePO}_4 \cdot 0.5\text{H}_2\text{O}$, are given in Fig. S4. XANES spectrum of CSO-0 (Fig. 1(c)) is very similar to the Ce^{4+} standard one (CeO_2), implying a sample mainly doped with Ce^{4+} . Then the progressive decrease of the Ce^{4+} band (at 5737 eV) and increase of the Ce^{3+} band (at 5726 eV) with the reduction duration for all samples (Fig. 1(c)) lead to a spectrum very similar to the Ce^{3+} standard for CSO-96 and confirm the observations in diffuse reflection. Moreover, in energy scale, the highest absorption edge was observed for the Ce^{4+} standard (CeO_2) and the samples absorption edges are continuously decreasing with the reduction (continuous evolution from Ce^{4+} to Ce^{3+} , see inset in Fig. 1(c)). Linear combination fit of the samples spectra, considering the non-reduced sample (CSO-0) as fully Ce^{4+} -doped and the sample reduced for 96h (CSO-96) as fully Ce^{3+} -doped, confirms the continuous increase of the Ce^{3+} ratio (Table 1). The XANES spectra of CSO-48 and its corresponding linear combination fit curve are presented as an example in Fig. S5.

Diffuse reflection and XANES measurement confirmed the presence of different Ce^{3+} ratios, increasing with the reduction duration, in the samples CSO-0 to CSO-96. Moreover, these results also suppose that the complete reduction of the Ce^{4+} in our samples should be obtained with a reduction duration around 96h. Ce^{3+} is referenced to substitute Ca^{2+} in CaSc_2O_4 [15] ($r(\text{Ce}^{3+}) = 1.28 \text{ \AA}$, $r(\text{Ca}^{2+}) = 1.26 \text{ \AA}$).[24] Moreover, $\text{CaSc}_2\text{O}_4:\text{Ce}$ presents a large photoluminescence emission band, characteristic of Ce^{3+} at a single Ca^{2+} site, that can be deconvoluted into two bands separated by around 0.25 eV as expected (Fig. S1). No additional emission band has been detected, even at low temperature.[15,19] However due to its ionic radius intermediate between the radii of Ca^{2+} and Sc^{3+} (see table 2), a question remains open on the substitution site of Ce^{4+} . To investigate more thoroughly this point, EXAFS

Table 1

Ce^{3+} ratios obtained from the XANES spectra of samples CSO-0 to CSO-96 by linear combination fit considering CSO-0 as fully Ce^{4+} -doped and CSO-96 as fully Ce^{3+} -doped

Sample	$\Phi(\text{Ce}^{3+})$ (%)
CSO-0	0
CSO-1	26
CSO-24	73
CSO-48	91
CSO-96	100

measurements were carried out at the cerium K edge on two standards (CeO_2 for Ce^{4+} and $\text{CePO}_4 \cdot 0.5\text{H}_2\text{O}$ for Ce^{3+}) and two 1.5% cerium-doped samples: a non-reduced one (CSO-1.5-0) and a strongly reduced one (CSO-1.5-red). The cerium doping was increased comparing to samples CSO-0 to CSO-96 in order to improve signal resolutions. After extraction of the EXAFS signals, the radial distribution functions (Fig. 1(d)) and the Ce-O distances (table 3) were obtained by Fourier transform and refinement. We can observe for the first coordination sphere (see inset in Fig. 1(d)) that all samples present only one Ce-O distance. The Ce^{4+} standard and CSO-1.5-0 present similar short Ce-O distances. This distance is significantly increased for the Ce^{3+} standard and CSO-1.5-red. This confirms once again non-reduced samples mainly doped with Ce^{4+} and strongly reduced samples mainly doped with Ce^{3+} . Moreover, a very good accuracy on the obtained fitted Ce-O distances (table 3) can be expected while the exact crystallographic Ce-O distance[25] has been obtained in this way for CeO_2 . The fitted Ce-O distance in CSO-1.5-red is very close to the average Ca-O distance in CaSc_2O_4 [20] (2.517 \AA and 2.513 \AA respectively), confirming the Ca substitution by Ce^{3+} . More interestingly, CaSc_2O_4 presenting average Ca-O distances (2.513 \AA [20]) longer than the fitted Ce-O distances in CeO_2 (2.346 \AA), a Ca^{2+} substitution by Ce^{4+} cannot explain the shorter fitted Ce-O distance for CSO-1.5-0 than for CeO_2 (see table 3). However, the average Sc-O distance in CaSc_2O_4 (2.121 \AA [20]) is shorter than the Ce-O distance in CeO_2 . Ce^{4+} presents a larger radius than Sc^{3+} (see table 2), thus the Ce-O distance in CSO-1.5-0 is longer than for Sc-O in CaSc_2O_4 (respectively 2.235 \AA and 2.121 \AA [20]). Hence, in CaSc_2O_4 , Ce^{4+} substitutes Sc^{3+} sites. In this case, Ce^{3+} and Ce^{4+} both substituting elements with different radii and valence states, their presence might induce defects (but in extremely low amounts regarding to the already very low initial Ce concentrations).[26]

Table 2

Ionic radii of Ca^{2+} , Sc^{3+} , Ce^{3+} and Ce^{4+} [24]

Ion	Coordination	Radius (\AA)
Ca^{2+}	8	1.26
Sc^{3+}	6	0.87
Ce^{3+}	8	1.28
Ce^{4+}	6	0.94
	8	1.11

Table 3

Fitted Ce-O distances obtained by refinement of the radial distribution functions for CeO_2 , $\text{CePO}_4 \cdot 0.5\text{H}_2\text{O}$, CSO-1.5-0 and CSO-1.5-red

Sample	Ce-O distance (Å)
CeO ₂	2.364
CePO ₄ ·0.5H ₂ O	2.519
CSO-1.5-0	2.235
CSO-1.5-red	2.517

In order to probe the impact of the different Ce³⁺ ratios on the luminescence properties, photoluminescence spectra of samples CSO-0 to CSO-96 have been recorded (Fig. 2(a)). All samples present a green emission with a broad band ranging from 450 nm to 675 nm with a maximum at 517 nm assigned to Ce³⁺ at the Ca site, as previously mentioned. The luminescence intensity of the non-reduced sample (CSO-0) turns out to be very low, but this characteristic green emission[15,19] evidences that Ce³⁺ can be stabilized in CaSc₂O₄ even in air, but in very low ratios, since no clear identification of Ce³⁺ was possible through diffuse reflection or XANES (see in Fig. 1 (b) and (c)). The luminescence intensity of the CSO samples can be greatly enhanced with reduction. Hence, the sample reduced for 24h (CSO-24) shows a photoluminescence intensity 32 times higher than the non-reduced sample (CSO-0). At the opposite, for longer reduction durations, the intensity of luminescence decreases until an intensity 1.6 times lower than CSO-24 for the sample reduced for 96h (Fig. 2(a)). This evolution was confirmed by measurements of the quantum yields (RT, $\lambda_{\text{exc}} = 445$ nm) Fig. 2(b)) starting at 12% for the non-reduced sample (CSO-0) increasing up to 70% for CSO-24 and finally decreasing to 48% for CSO-96. PLQY measurements for all samples are presented in table S2. This behavior is similar to what can be commonly obtained with samples doped with different activator concentrations (with an optimal value leading to the highest emission intensity). However, here all samples were initially prepared with the same Ce concentration but were reduced for different durations.

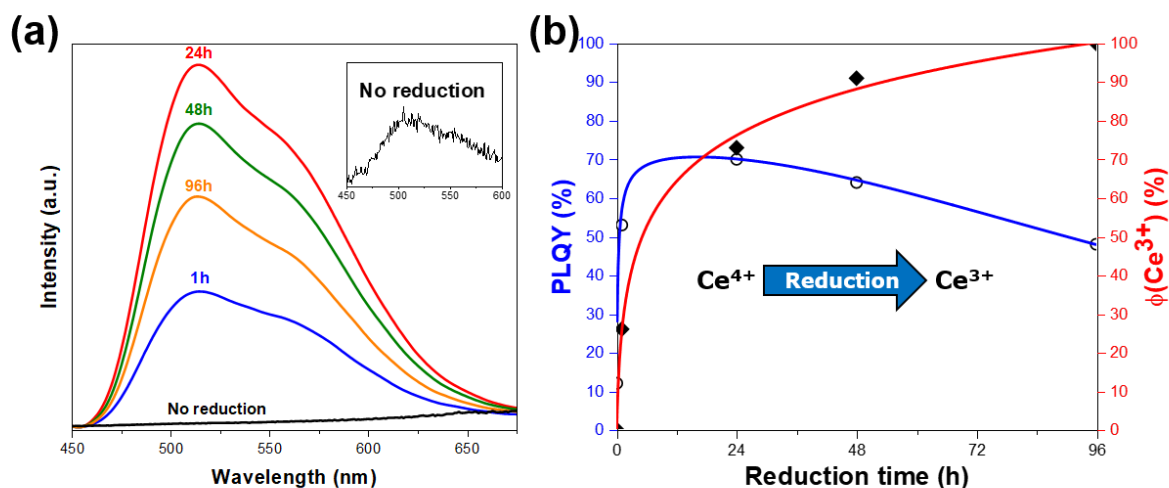


Fig. 2. (a) Solid-state photoluminescence spectra recorded at RT and $\lambda_{\text{exc}} = 445$ nm, for CSO-0 to CSO-96. (b) Plot of the photoluminescence quantum yields recorded at RT and $\lambda_{\text{exc}} = 445$ nm (white circles) and plot of the Ce³⁺ ratios obtained by linear combination fit from the XANES spectra (black rhombi) for CSO-0 to CSO-96 (fitting curves are added to guide the eye).

Although cerium doped materials are commonly highly reduced, our results show here that strong reduction might not always be appropriate to obtain the highest efficiencies of luminescence. As an example, the best efficiency for CaSc₂O₄:Ce has been previously reported to be reached with supposed fully reduced materials (due to the reduction conditions) doped with 0.5% of cerium.[15] Here, the best efficiency for CaSc₂O₄ doped with 0.5% of cerium was obtained with a partially reduced sample. This suggests that the optimal doping for this material is below 0.5%.

At first sight, the increase of the photoluminescence efficiency with reduction is more likely due to the increase of the Ce³⁺ ratio. Even though all samples present comparable peak widths (Fig. S3), a slight signal to noise ratio improvement is observed for longer annealings (from 24h to 96h). Thus, a slight increase of the samples crystallinity could also improve their photoluminescence intensity. However, the samples microstructure remains the same for all samples presenting a decrease of their photoluminescence properties (CSO-24 to 96). This behavior then observed could be associated to a concentration quenching phenomenon while the Ce³⁺ total ratio is still increased by reduction. If such a de-excitation mechanism takes place, non-radiative transitions are

expected between Ce^{3+} cations separated by a distance lower than a critical distance R_c , described by the Equ.1.[27]:

$$R_c^6 = 3.10^{12} \times f_a \times E^{-4} \times \text{SO} \quad (1)$$

where f_a is the broad $4f \rightarrow 5d^1$ absorption band oscillator strength (taken at 10^{-2} from Blasse[27]), E the energy of maximum spectral overlap and SO the spectral overlap integral between the normalized emission and excitation spectra (found at 2.59 eV and $2.86 \cdot 10^{-2} \text{ eV}^{-1}$ respectively). Based on the Equ. 1, the Ce^{3+} - Ce^{3+} critical distance in CaSc_2O_4 is estimated around $R_c = 16 \text{ \AA}$. Based on the Dexter formula,[6,27] the theoretical optimal doping (X_c), before concentration quenching, can then be determined (Equ.2):

$$X_c = \frac{6V}{4\pi N R_c^3} \quad (2)$$

where V is the unit cell volume ($V = 330.3 \text{ \AA}^3$ [20]) and N the number of sites in the unit cell that can host Ce^{3+} cations ($N = 4$). For $\text{CaSc}_2\text{O}_4:\text{Ce}$, the optimal doping, before concentration quenching, is calculated at $X_c = 0.9\%$ for Ce^{3+} at the Ca site. However, as previously mentioned, the best efficiency has been obtained here with a partially reduced sample doped with 0.5% of cerium. Therefore, the origin of the efficiency decrease in $\text{CaSc}_2\text{O}_4:\text{Ce}$ cannot originate from concentration quenching.

Another mechanism could explain the photoluminescence intensity decrease in $\text{CaSc}_2\text{O}_4:\text{Ce}$ for long reduction treatments. Thus, George et al., suggested that the high efficiency of $\text{CaSc}_2\text{O}_4:\text{Ce}$ could originate from its high structural rigidity. Nevertheless, the increase of the Ce^{3+} concentration would lead, beyond a given threshold value, to local distortions that could enhance the probability of non-radiative relaxation.[15] In that context, it is important to notice that only very small local distortions would be responsible for the photoluminescence quenching. Thus, no significant changes can be observed on the cell parameters of all samples (table S1) or PXRD peaks width (for samples CSO-24 to CSO-96). Nevertheless, as previously mentioned, Ce^{4+} and Ce^{3+} substitute Sc and Ca sites respectively. Therefore, the reduction of Ce^{4+} into Ce^{3+} will lead to an increase of Ca substitutions in the materials that can be assimilated to an increase of the Ce^{3+} doping at the Ca site as described by George *et al.*[15] Thus, the reduction could bring, in the same way, more local distortions at or around the Ce^{3+} site, leading to more non-radiative relaxation and a decrease of the photoluminescence efficiency above a given Ce^{3+} concentration. However, due to the absence of significant differences between samples CSO-0 to 96 regarding to their microstructures (see in Fig. S3 and Table S1), this latter quenching mechanism cannot be confirmed here.

Different heating treatments can impact the phosphors emission properties for example by leading to different crystallizations. Nevertheless, the photoluminescence evolution of $\text{CaSc}_2\text{O}_4:\text{Ce}$ with reduction is here only influenced by the Ce^{3+} ratios since samples CSO-0 to 96 present comparable crystallinities (no differences in the PXRD patterns for CSO-24 to 96) and the same cerium doping (0.5%). Moreover, the absence of excitation band at the working wavelength (445 nm) for the non-reduced sample in diffuse reflection (Fig. 1(b)) suggests that the presence of Ce^{4+} should not bring any direct luminescence properties. Furthermore, Ce^{3+} and Ce^{4+} substitute different sites (Ca^{2+} and Sc^{3+} , respectively), presenting lower charge than the dopants (in both cases a +1 charge difference is observed). Therefore, we believe that all sample should present the same defects, because the same charge imbalance could be observed in any case. Moreover, at low temperature, the materials Ce^{3+} emission follows a common decrease of its emission intensity with the increase of the temperature (see Fig. S6 for CSO-24). No additional phenomenon is observed at low temperature implying possible defects presenting an impact on the photoluminescence properties of the materials. While the total Ce^{3+} ratio is constantly increasing, the luminescence properties evolution of $\text{CaSc}_2\text{O}_4:\text{Ce}$ with reduction presents an increase followed by a decrease of its efficiency (Fig. 2(a) and (b)). However, due to the low difference between the Ce concentration in all samples (0.5%) and the calculated value for Ce^{3+} before concentration quenching ($X_c = 0.9\%$), this possible mechanism might not be excluded. Taking all of this into account, a reduction mechanism could be proposed by focusing on the evolution of the Ce^{3+} ratio ($\Phi(\text{Ce}^{3+})$, percentage of Ce^{3+} over the whole cerium amount) and its impact on the photoluminescence properties.

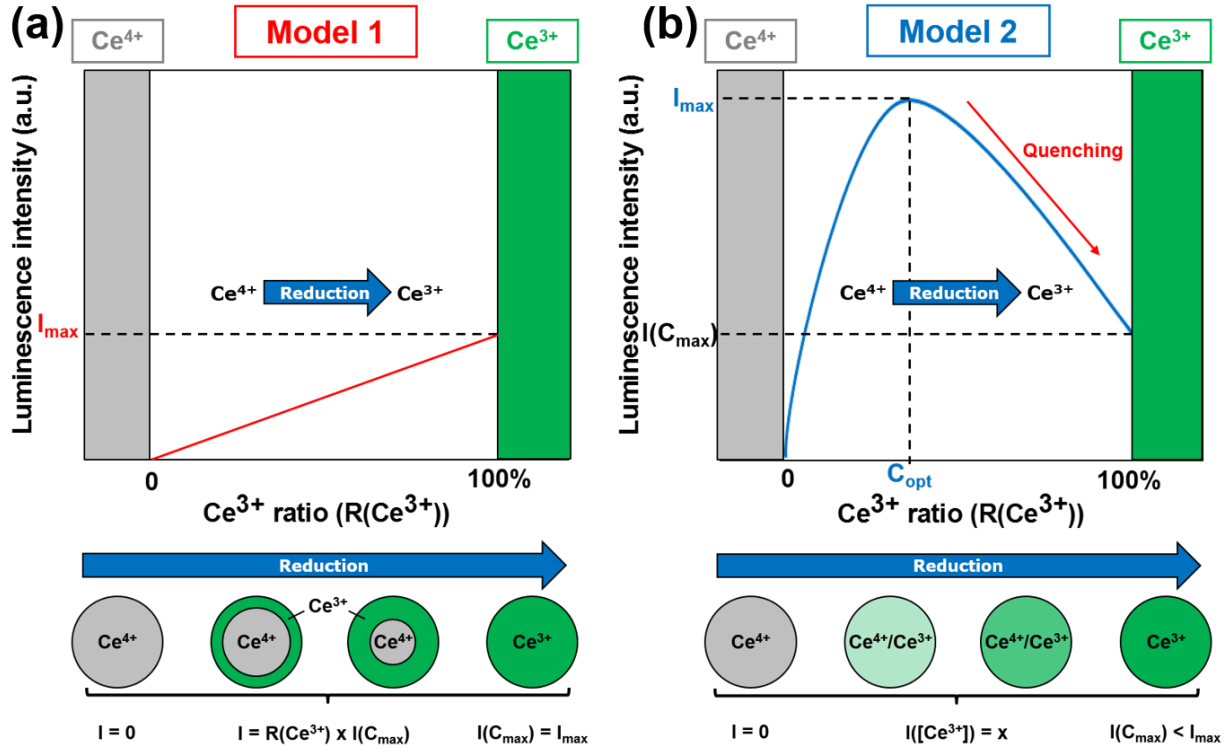


Fig. 3. Schemes of the (a) heterogeneous (model 1) and (b) homogeneous (model 2) reductions for cerium-doped phosphors. Grey color represents Ce^{4+} -doped volumes, green color Ce^{3+} -doped volumes and lighter green colors $\text{Ce}^{3+}/\text{Ce}^{4+}$ mixed valence volumes.

A first model (model 1, Fig. 3(a)) would consist in the formation of two distinguishable phases with reduction, one fully doped with Ce^{4+} (P_1 , with $\Phi(\text{Ce}^{3+}) = 0\%$) and the other one fully doped with Ce^{3+} (P_2 , with $\Phi(\text{Ce}^{3+}) = 100\%$) (e.g. non-reduced and reduced grains or core-shell reduction, Fig. 3(a)). As Ce^{4+} ions do not play the role of activator, only the Ce^{3+} -doped phase (P_2) would provide luminescence. Therefore, reduction would lead to the growth of P_2 at the detriment of P_1 and the luminescence intensity would increase linearly until a specific value ($I(C_{\max}) = I_{\max}$) characteristic of the total cerium concentration in the sample (C_{\max}) (Equ.3):

$$I = \Phi(\text{Ce}^{3+}) \times I(C_{\max}) \quad (3)$$

In this model, the effects of the excitation beam penetration and self-absorption phenomenon are not taken into account, because they would only impact the curve slope to reach I_{\max} . This model can be assimilated to heterogeneously (or biphasic) distributed Ce^{3+} and Ce^{4+} in the volume leading to a continuous increase of the luminescence intensity, limited to a maximum (I_{\max}) characteristic of the total cerium concentration in the material (C_{\max}). Nevertheless, in our study, $\text{CaSc}_2\text{O}_4:\text{Ce}$ does not present such evolution of its intensity with reduction but an increase followed by a decrease.

A second model (model 2, Fig. 3(b)) would consist in a homogeneous distribution of Ce^{3+} and Ce^{4+} in the volume (one single phase codoped with Ce^{3+} and Ce^{4+}), with the luminescence intensity depending on the Ce^{3+} concentration. In this model, the increase of the Ce^{3+} ratio ($\Phi(\text{Ce}^{3+})$) by reduction would first lead to an increase of the luminescence intensity. Then, a maximum value (I_{\max}) would be obtained when reaching the optimal Ce^{3+} concentration (C_{opt}). Finally, the Ce^{3+} ratio would continue to increase with reduction but a decrease of the intensity of luminescence should be observed due to a quenching (in our case because of distortions[15]) until a value $I(C_{\max}) < I_{\max}$ (Equ.4):

$$I = I(\Phi(\text{Ce}^{3+}) \times C_{\max}) \quad (4)$$

with $0 \leq I \leq I_{\max}$ when $\Phi(\text{Ce}^{3+}) \times C_{\max} \leq C_{\text{opt}}$ and $I_{\max} \geq I \geq I(C_{\max})$ when $\Phi(\text{Ce}^{3+}) \times C_{\max} \geq C_{\text{opt}}$. In our case $C_{\max} = 0.5\%$, hence $C_{\text{opt}} < 0.5\%$. Even though an intermediate mechanism between both models is possible, to explain the behavior of $\text{CaSc}_2\text{O}_4:\text{Ce}$, the reduction mechanism should be closer to the one described in the second model.

4. Conclusion

The control of doped materials properties is ruled by many well-known parameters, such as doping concentration, synthesis temperature, grain size or crystallinity. Our work shows that even though it is not much

considered, the ratios of dopants in different oxidation states is also of high importance since a mixed valence of dopants can be present for syntheses in air and even in reducing atmosphere. In this study, we demonstrated that the photoluminescence intensity of $\text{CaSc}_2\text{O}_4:\text{Ce}$ can be increased up to 32 times owing to a partial reduction, but a decrease of its efficiency (PLQY from 70% to 48%) will be observed by increasing the reduction duration. This highlights the drastic impact of reduction on photoluminescence properties and shows that strong reductions might not always be ideal to reach the best efficiencies. Moreover, our work shows that cerium-doped phosphors can be assimilated to single phases codoped with Ce^{3+} and Ce^{4+} (homogeneous distribution of Ce^{4+} and Ce^{3+} in the material) because of the continuous increase of the Ce^{3+} ratio and the observed quenching of the $\text{CaSc}_2\text{O}_4:\text{Ce}$ efficiency after long reduction durations. Furthermore, we believe that these results are also of high interest for any materials with multivalent dopant (such as Eu, Mn, Cu, Ni or Fe) because these latter can present very different properties depending on their stabilized oxidation state (for example different emission colors with Eu^{3+} or Eu^{2+}). Since reduction leads to a homogeneous distribution of the dopants with different oxidation states in the materials, these results are of great importance for the control of a high diversity of tunable properties such as luminescence, absorption, conductivity or magnetism. The better understanding of the dopants reduction mechanism and its control will help improving a large variety of applications, among them: LEDs, sensors, transparent semi-conductors, bio-imaging.

Associated content

Supplemental Information includes: Solid-state photoluminescence spectrum deconvolution of sample CSO-24; Rietveld refinements of all other samples; Normalized PXRD patterns and cell parameters of samples CSO-0 to 96; Solid-state photoluminescence spectra of sample CSO-24 recorded at temperatures ranging from 77K to 500K; Normalized XANES spectra of the Ce^{3+} and Ce^{4+} standards; Normalized XANES spectrum of sample CSO-48 and its corresponding linear combination fit; Measured quantum yields for samples CSO-0 to 96. This material is available free of charge via the Internet.

Conflict of interest

The authors declare no competing financial interests.

Acknowledgments

Authors thank synchrotron SOLEIL for providing the synchrotron radiation facilities (Proposal 20180647) as well as Dr. Emiliano Fonda and Dr. Camille Lafontaine for their valuable help on the XANES and EXAFS characterizations on the Samba and Rock beamlines respectively. Authors also thank Dr. Abdel Mesbah for providing the $\text{CePO}_4 \cdot 0.5\text{H}_2\text{O}$ sample.

References

- [1] P. Pust, P.J. Schmidt, W. Schnick, A revolution in lighting, *Nature Materials*. 14 (2015) 454–458. <https://doi.org/10.1038/nmat4270>.
- [2] Solid-State Lighting 2017 R&D Plan: Suggested Research Topics | Department of Energy, (n.d.). <https://www.energy.gov/eere/ssl/downloads/solid-state-lighting-2017-rd-plan-suggested-research-topics> (accessed November 20, 2018).
- [3] W. Manager, Energy Savings Forecast of Solid-State Lighting in General Illumination Applications • National Lighting Bureau (NLB), National Lighting Bureau (NLB). (2017). <https://nlb.org/energy-savings-forecast-of-solid-state-lighting-in-general-illumination-applications-2/> (accessed November 20, 2018).
- [4] V. Bachmann, C. Ronda, A. Meijerink, Temperature Quenching of Yellow Ce^{3+} Luminescence in YAG:Ce, *Chem. Mater.* 21 (2009) 2077–2084. <https://doi.org/10.1021/cm8030768>.
- [5] N.C. George, K.A. Denault, R. Seshadri, Phosphors for Solid-State White Lighting, *Annual Review of Materials Research*. 43 (2013) 481–501. <https://doi.org/10.1146/annurev-matsci-073012-125702>.
- [6] W.B. Im, S. Brinkley, J. Hu, A. Mikhailovsky, S.P. DenBaars, R. Seshadri, $\text{Sr}_{2.975-x}\text{Ba}_x\text{Ce}_{0.025}\text{AlO}_4\text{F}$: a Highly Efficient Green-Emitting Oxyfluoride Phosphor for Solid State White Lighting, *Chem. Mater.* 22 (2010) 2842–2849. <https://doi.org/10.1021/cm100010z>.
- [7] Y. Shimomura, T. Honma, M. Shigeiwa, T. Akai, K. Okamoto, N. Kijima, Photoluminescence and Crystal Structure of Green-Emitting $\text{Ca}_3\text{Sc}_2\text{Si}_5\text{O}_{12}:\text{Ce}^{3+}$ Phosphor for White Light Emitting Diodes, *J. Electrochem. Soc.* 154 (2007) J35–J38. <https://doi.org/10.1149/1.2388856>.
- [8] S.K. Sharma, Y.-C. Lin, I. Carrasco, T. Tingberg, M. Bettinelli, M. Karlsson, Weak thermal quenching of the luminescence in the $\text{Ca}_3\text{Sc}_2\text{Si}_5\text{O}_{12}:\text{Ce}^{3+}$ garnet phosphor, *J. Mater. Chem. C*. 6 (2018) 8923–8933. <https://doi.org/10.1039/C8TC02907E>.
- [9] L. Wang, L. Zhuang, H. Xin, Y. Huang, D. Wang, Semi-Quantitative Estimation of $\text{Ce}^{3+}/\text{Ce}^{4+}$ Ratio in YAG:Ce³⁺ Phosphor under Different Sintering Atmosphere, *Open Journal of Inorganic Chemistry*. 05 (2015) 12. <https://doi.org/10.4236/ojic.2015.51003>.
- [10] Y. Pan, M. Wu, Q. Su, Tailored photoluminescence of YAG:Ce phosphor through various methods, *Journal of Physics and Chemistry of Solids*. 65 (2004) 845–850. <https://doi.org/10.1016/j.jpcs.2003.08.018>.

- [11] Y. Liu, W. Zhuang, Y. Hu, W. Gao, Improved photoluminescence of green-emitting phosphor $\text{Ca}_3\text{Sc}_2\text{Si}_3\text{O}_{12}:\text{Ce}^{3+}$ for white light emitting diodes, *Journal of Rare Earths*. 28 (2010) 181–184. [https://doi.org/10.1016/S1002-0721\(09\)60076-4](https://doi.org/10.1016/S1002-0721(09)60076-4).
- [12] G. Kaur Behrh, H. Serier- Brault, S. Jobic, R. Gautier, A Chemical Route Towards Single-Phase Materials with Controllable Photoluminescence, *Angewandte Chemie*. 127 (2015) 11663–11665. <https://doi.org/10.1002/ange.201504224>.
- [13] R. Gautier, X. Li, Z. Xia, F. Massuyeau, Two-Step Design of a Single-Doped White Phosphor with High Color Rendering, *J. Am. Chem. Soc.* 139 (2017) 1436–1439. <https://doi.org/10.1021/jacs.6b12597>.
- [14] H. Barroux, T. Jiang, C. Paul, F. Massuyeau, R. Géniois, E.E. Gordon, M.-H. Whangbo, S. Jobic, R. Gautier, Fine-Tuning the Properties of Doped Multifunctional Materials by Controlled Reduction of Dopants, *Chemistry – A European Journal*. 23 (2017) 2998–3001. <https://doi.org/10.1002/chem.201605707>.
- [15] N.C. George, J. Brgoch, A.J. Pell, C. Cozzan, A. Jaffe, G. Dantelle, A. Llobet, G. Pintacuda, R. Seshadri, B.F. Chmelka, Correlating Local Compositions and Structures with the Macroscopic Optical Properties of Ce^{3+} -Doped CaSc_2O_4 , an Efficient Green-Emitting Phosphor, *Chem. Mater.* 29 (2017) 3538–3546. <https://doi.org/10.1021/acs.chemmater.6b05394>.
- [16] J.C. de Mello, H.F. Wittmann, R.H. Friend, An improved experimental determination of external photoluminescence quantum efficiency, *Advanced Materials*. 9 (1997) 230–232. <https://doi.org/10.1002/adma.19970090308>.
- [17] B. Ravel, M. Newville, ATHENA, ARTEMIS, HEPHAESTUS: data analysis for X-ray absorption spectroscopy using IFEFFIT, *J Synchrotron Radiat.* 12 (2005) 537–541. <https://doi.org/10.1107/S0909049505012719>.
- [18] T. Ressler, WinXAS : A New Software Package not only for the Analysis of Energy-Dispersive XAS Data, *J. Phys. IV France*. 7 (1997) C2-269-C2-270. <https://doi.org/10.1051/jp4/1997195>.
- [19] S.K. Sharma, M. Bettinelli, I. Carrasco, M. Karlsson, Influence of Ce^{3+} Concentration on the Thermal Stability and Charge-Trapping Dynamics in the Green Emitting Phosphor $\text{CaSc}_2\text{O}_4:\text{Ce}^{3+}$, *J. Phys. Chem. C*. 121 (2017) 23096–23103. <https://doi.org/10.1021/acs.jpcc.7b08263>.
- [20] R. Horyn, Lukaszew.k, Refinement of Crystal Structure of CaSc_2O_4 , *Bulletin De L'Académie Polonaise Des Sciences-Série Des Sciences Chimiques*. 14 (1966) 499-504.
- [21] F. Goubin, X. Rocquefelte, M.-H. Whangbo, Y. Montardi, R. Brec, S. Jobic, Experimental and Theoretical Characterization of the Optical Properties of CeO_2 , SrCeO_3 , and Sr_2CeO_4 Containing Ce^{4+} (f_0) Ions, *Chem. Mater.* 16 (2004) 662–669. <https://doi.org/10.1021/cm034618u>.
- [22] X.-Y. Sun, Z.-H. Xiao, Y.-T. Wu, X.-G. Yu, Q.-L. Hu, Y. Yuan, Q. Liu, C. Struebing, Z. Kang, Role of Al^{3+} on tuning optical properties of Ce^{3+} -activated borosilicate scintillating glasses prepared in air, *Journal of the American Ceramic Society*. 101 (2018) 4480–4485. <https://doi.org/10.1111/jace.15773>.
- [23] S.M. Loureiro, Y. Gao, V. Venkataramani, Stability of Ce(III) Activator and Codopant Effect in MHfO_3 (M=Ba, Sr) Scintillators by XANES, *Journal of the American Ceramic Society*. 88 (2005) 219–221. <https://doi.org/10.1111/j.1551-2916.2004.00004.x>.
- [24] R.D. Shannon, C.T. Prewitt, Effective ionic radii in oxides and fluorides, *Acta Cryst B*. 25 (1969) 925–946. <https://doi.org/10.1107/S0567740869003220>.
- [25] R. Sharan, A. Dutta, Structural analysis of Zr^{4+} doped ceria, a possible material for ammonia detection in ppm level, *Journal of Alloys and Compounds*. 693 (2017) 936–944. <https://doi.org/10.1016/j.jallcom.2016.09.267>.
- [26] W.-L. Feng, C.-Y. Tao, K. Wang, Synthesis and Photoluminescence of Tetravalent Cerium-Doped Alkaline-Earth-Metal Tungstate Phosphors by a Co-precipitation Method, *Spectroscopy Letters*. 48 (2015) 381–385. <https://doi.org/10.1080/00387010.2014.890941>.
- [27] G. Blasse, B.C. Grabmaier, *Luminescent Materials*, Springer-Verlag, Berlin Heidelberg, 1994. <https://www.springer.com/fr/book/9783540580195> (accessed March 4, 2019).